JOURNAL OF THERMOPHYSICS AND HEAT TRANSFER
Vol. 18, No. 3, July–September 2004

Thermal Transport in High Porosity Cellular Metal Foams

C. Y. Zhao,* T. Kim,* T. J. Lu,† and H. P. Hodson‡
University of Cambridge, Cambridge, England CB2 1PZ, United Kingdom

The heat dissipation capability of highly porous cellular metal foams with open cells subject to forced air convection is studied using a combined experimental and analytical approach. The cellular morphologies of six FeCrAlY (an iron-based alloy) foams and six copper alloy foams with a range of pore sizes and porosities are quantified with the scanning electronic microscope and image analysis. Experimental measurements on pressure drop and heat transfer for copper foams are carried out. A numerical model for forced convection across open-celled metal foams is subsequently developed, and the predictions are compared with those measured. Reasonably good agreement with test data is obtained, given the complexity of the cellular foam morphology and the associated momentum/energy transport. The results show that cell size has a more significant effect on the overall heat transfer than porosity. An optimal porosity is obtained based on the balance between pressure drop and overall heat transfer, which decreases as the Reynolds number is increased.

Nomenclature

$\tilde{a}$	=	specific surface area per unit volume
C_f	=	heat capacity of fluid
C_I	=	inertial coefficient
d_f	=	diameter of cell edge ligament
d_p	=	pore size
F_I	=	inertial variable
f	=	friction factor
H	=	channel height
h_{sf}	=	interfacial heat transfer coefficient
$\bar{h}$	=	overall heat transfer coefficient
K	=	permeability
k_f	=	thermal conductivity of fluid
k_{fe}	=	effective thermal conductivity of fluid
k_s	=	thermal conductivity of solid
k_{se}	=	effective thermal conductivity of solid
L, L_m	=	length of channel, momentum length scale
Nu_x	=	local Nusselt number
$\overline{Nu}$	=	overall Nusselt number
P	=	pressure
Pr	=	Prandtl number
q_w	=	heat flux over bottom surface of channel
r	=	inner-to-outer ligament diameter ratio
T	=	temperature
T_f	=	fluid temperature
T_{in}	=	inlet fluid temperature
T_s	=	solid temperature
T_w	=	bottom wall temperature
u	=	velocity
ε	=	porosity
ε_{opt}	=	optimal porosity
μ_f	=	viscosity of fluid
ρ_f	=	density of fluid

Received 13 February 2003; revision received 17 September 2003; accepted for publication 1 December 2003.

*Ph.D. Student, Department of Engineering, Trumpington Street.
†Reader, Department of Engineering, Trumpington Street; TJL21@cam.ac.uk.
‡Professor, Department of Engineering, Trumpington Street.

Introduction

HIGH porosity (>90%) cellular metal foams with open cells (Fig. 1) have emerged in recent years as one of the most promising materials for thermal management applications where a large amount of heat needs to be transported over a small volume. The motivation is attributed to the high surface area to volume ratio, as well as enhanced flow mixing due to the tortuosity of metal foams. Furthermore, metallic foams have attractive stiffness/strength properties and can be processed in large quantity at low cost via the metal sintering route. The distinctive feature of metal foams thus processed is that the cell edge struts (ligaments) are hollow (inset in Fig. 1), in contrast with the solid struts of metal foams manufactured via the more expensive investment casting route, for example, Duocell® foam from ERG Company, California.

From the heat transfer point of view, even though metal foams can be broadly classified as porous media, they have very distinctive features such as high porosities and a unique open-celled morphology. Consequently, most of previous studies on packed beds and granular porous media with a porosity range of 0.3–0.6 are not directly applicable to metal foams. It is only during the past 15 years, that transport phenomena in open-celled metal foams with solid-cell ligaments have started to receive attention.[1–11] Under the assumption of local thermal equilibrium, Hunt and Tien[1] studied the effects of thermal dispersion on forced convection in metal foams with water as the fluid phase. They concluded that the conduction of a metal foam may not be significant due to its thin cell ligaments and that dispersion may dominate the heat transport. Sathe et al.[2] studied combustion in metal foams as applied to porous radiant burners. Younis and Viskanta[3] measured the volumetric heat transfer of ceramic foam materials and developed a Nusselt number correlation fit to the experimental data. The volumetric heat transfer rates measured were higher than those for packed beds. Lee et al.[4] investigated the application of metal foams as high-performance air-cooled heat sinks in electronics packaging and found experimentally that aluminum foams could dissipate heat fluxes up to 100 W/cm^2.

With the metal foams idealized as interconnected cylinders, Lu et al.[5] developed an analytical model to predict their heat dissipation capability under forced convection. Bastarows et al.[6] studied single-sided heating of a foam-filled plate channel for electronics cooling applications. ERG (Duocel) aluminum foams were used. The experimental method utilized both conductive thermal epoxy bonding and brazing of the metal foam to a heated plate. The results revealed that brazed-foam samples are much more effective at heat removal than epoxy-bonded samples, with the former capable of removing three times more heat than a conventional fin–pin array. Calmidi and Mahajan,[7,8] proposed an effective thermal conductivity model for metal foams having idealized cellular structures and conducted an experimental and numerical investigation on forced

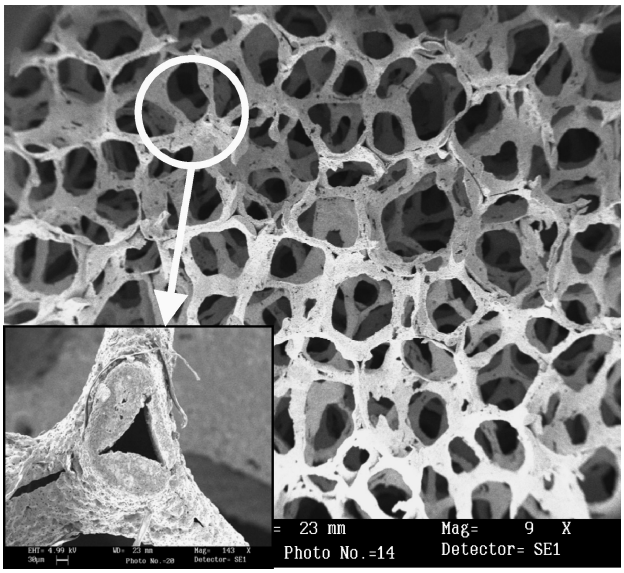

Fig. 1 Typical Porvair FeCrAlY foam: cellular morphology and cross section of an individual strut.

air convection in ERG aluminum foams. In their numerical study, the two-equation heat transfer model was employed, and it is found that thermal dispersion effect is extremely small if the fluid phase is air, in contrast with the conclusion derived by Hunt and Tien[1] with water as the coolant. Kim et al.[9] experimentally studied laminar heat transport in ERG aluminum foams and found that the foam offers a better heat transfer performance compared to that of a louvered array, albeit at a greater pressure drop. The effective conductivity and permeability of ERG aluminum foams were studied by Paek et al.[10] and Boomsma and Poulikakos.[11]

Although a number of investigations have focused on the transport of heat in open-celled foams,[1–11] the study is still incomplete. First, because ceramic or aluminum foams with solid cell struts are the focus of previous studies, for forced convection across metal foams made of different materials, for example, copper and a high-temperature steel alloy, FeCrAlY (73-wt% Fe, 20-wt% Cr, 5-wt% Al, and 2-wt% Y), with different cellular morphologies, there is little information in the open literature, and there is a lack of reliable experimental data. Second, various models on the effective thermal conductivity of metal foams have been proposed,[7,10,11] but how these models can be used to predict the overall heat transfer performance of the foam in forced convection remains to be quantitatively studied. Third, in the present study, the coolant velocity varies over one order of magnitude, and so the flow may span different regimes (viscous dominated as opposed to form dominated). Thus, the hydraulic behavior and flow regime need to be determined to examine properly the momentum equation used in the modeling. Finally, the effects of microstructural parameters, for example, porosity, pore size, and inner-to-outer ligament diameter ratio, on the overall foam heat transfer need to be determined.

The aim of this paper is first to use the scanning electronic microscope (SEM) and image analysis to characterize the microstructures of metal foams manufactured by Porviar Fuel Cell Technology (Hendersonville, North Carolina) with the sintering route and then to measure pressure drop and overall heat transfer properties for foam samples having different porosities and cell sizes. The independent parameters characterizing the morphologies of the metal foams are to be determined. The momentum equation will then be examined and a formulation for form coefficient proposed to cover the high-velocity range. A numerical model will subsequently be developed for forced convective heat transfer in Porvair foams, incorporating the measured microstructural parameters. The effects of varying foam parameters on the overall heat transfer performance of a foam-filled plate channel will be studied in detail. This paper is an extended version of Ref. 12 (Zhao et al.), with experimental details added.

Microstructure of Porvair Metal Foams

Specifications of Cell and Foam Parameters

A typical Porvair metal foam structure shown in Fig. 1 is characterized by several key geometrical and physical parameters, namely, porosity ε (void volume fraction), pore size d_p, cell edge ligament diameter d_f, inner-to-outer ligament diameter ratio r, and relative density ρ_r. Note that these parameters are not all independent of each other, and their cross relationships will be examined later.

Cell Morphology Measurement

The pore size, ligament diameter, relative density, and inner-to-outer diameter ratio of the ligament were measured for both FeCrAlY and copper Porvair foam samples. The as-received samples have been specified with industrial terminologies: pore size in terms of pores per inch (PPI) (standard industrial specification of pore size) and relative density. Tables 1 and 2 list all samples and their industrial specifications. The measurement of cell and foam parameters was conducted by combining the SEM and the image analysis software KS 400 version 3.0 (Karl Zeiss Vision, GmbH). To obtain good images with the SEM, the electrical discharge machine was used to cut each sample, providing a good quality cutting section with smooth surfaces. For each sample, 20 or more SEM images were taken. For each sample, at least 10 cells were measured to calculate the averaged cell size with its standard deviation. The relative density was obtained by weighing the foam sample (kept in a vacuum chamber for 24 h before measurement) and measuring its overall dimensions.

Results of Measured Microstructures

The measured microstructures (cell size, relative density, and ligament diameter) are listed in Tables 1 and 2 together with the corresponding nominal cell sizes and relative densities. Notice that there

Table 1 Measured cell and foam parameters for FeCrAlY samples

	Sample number					
Properties	S-1	S-2	S-3	S-4	S-5	S-6
PPI	10	10	30	30	60	60
Nominal relative density, %	5	10	5	10	5	10
Measured relative density, %	5.7	14.3	6.1	10.2	9.0	13.7
Measured relative density, core only, %	4.6	12.5	4.1	9.3	5.5	9.2
Nominal cell size, mm	2.54	2.54	0.847	0.847	0.423	0.423
Measured cell size, mm	3.131	3.109	1.999	2.089	0.975	0.959
Hole diameter, μm	161	154	110	107	43.5	41.6
Fiber diameter, μm	287	351	215	267	124	154
Ratio, %	56	44	51	40	35	27

Table 2 Measured cell and foam parameters for copper samples

	Sample number					
Properties	S-7	S-8	S-9	S-10	S-11	S-12
PPI	10	10	30	30	60	60
Nominal relative density, %	5	10	5	10	5	10
Measured relative density, %	6.7	8.2	4.4	10.0	5.7	9.5
Measured relative density, core only, %	7.44	11.5	6.0	11.9	7.3	8.5
Nominal cell size, mm	2.54	2.54	0.847	0.847	0.423	0.423
Measured cell size, mm	2.645	2.697	1.284	1.431	0.554	0.657
Hole diameter, μm	n/a	n/a	n/a	n/a	n/a	n/a
Fiber diameter, μm	263	270	122	127	88.8	93.2
Hole-to-fiber diameter ratio, %	n/a	n/a	n/a	n/a	n/a	n/a

is significant difference between the nominal and measured cell sizes and that the cell size of a FeCrAlY sample is quite different from that of a copper sample that having identical PPI and relative density specifications. The difference may be attributed to the manufacturing process (metal sintering) and the properties of different materials. The other parameters to be measured from the SEM images are the inner and external diameters of cell edge ligaments. For FeCrAlY samples, reasonably good measurements can be made because the images taken for various hollow struts have relatively good quality. For copper samples, however, SEM images reveal that nearly all of the struts are solid, with no visible presence of inner holes. This has been attributed to the more complete sintering process of copper ligaments after the evaporation of the polymeric skeleton. Consequently, only the averaged ligament diameters were measured for copper samples.

The foam samples used in the heat transfer experiments are of the sandwich type, consisting of a foam core brazed onto two thin copper plates. Depending on the quality of processing and the material being used, the weight of the brazing material could take up a considerable portion of the weight of the foam itself. Therefore, two relative densities were measured for each sample. The first measurement represents the relative density of the whole foam core (including the brazing material). To minimize the effect of brazing, a second measurement was made by cutting a small cubic sample from the central portion of the foam core. Substantial discrepancy exists between the two relative densities for a given sample (Table 2). Interestingly, the first measurement is consistently larger than the second measurement for FeCrAlY samples, whereas the reverse holds for copper samples. This indicates that, whereas there is a high concentration of brazing material near the foam–plate interface for FeCrAlY samples, the residues of the brazing material have somehow migrated from the interface to the central portion of the foam core in copper samples. However, given the high porosity (>90%) of the metal foams studied, it is believed that the brazing process may only have negligibly small effect on the open pore spaces.

Length Scale

To analyze the experimental and/or numerical results for the fluid flow and heat transfer in a nondimensional way, a proper length scale needs to be identified. The mechanisms of fluid flow and heat transfer in porous media are significantly different, even though they are intrinsically coupled together (if the variation of fluid properties with temperature is accounted for). At a given velocity, the hydraulic behavior (pressure drop) mainly depends on the microstructure of the porous media, and it is essentially independent of the macrolength scale such as the channel height (for a two-dimensional problem) or hydraulic diameter (for a three-dimensional problem). However, the same cannot be said about heat transfer, which not only depends on the microstructure of the porous media but also, perhaps more important, on the channel height or hydraulic diameter. Furthermore, as far as the overall heat transfer in porous media is concerned, the total amount of surface area (related to the channel height or hydraulic diameter) is expected to play a more important rule than microstructural details. The length scales should, therefore, be different for momentum and thermal behaviors.

Various momentum length scales such as the channel height, pore diameter, particle diameter, or square-root of the permeability have been used by different researchers, often without clear justifications or explanations. Lage[13] indicated that the discussed momentum length scales all lack theoretical base, and they can lead to confusions when estimating the transition from viscous-dominated flow to form-dominated flow. For high Reynolds number fluid flows in porous media, Lage[13] argued that the ratio of the viscous force (linear Darcy term, $\mathrm{D}_\mu = \mu U/K$) and the form force (nonlinear term, $\mathrm{D}_F = \rho F_I U^2$) could be a more sensible alternative to estimate the flow regime transition and hydraulic behavior,

$$\frac{\mathrm{D}_F}{\mathrm{D}_\mu} = \frac{\rho F_I U^2}{(\mu/K)\,U} = \frac{\rho F_I K U}{\mu} \tag{1}$$

where K is the permeability of the porous medium (in square meters) and F_I is the form coefficient (per meter). A proper momentum length scale can be determined from Eq. (1), as

$$L_m = F_I K \tag{2}$$

The form coefficient F_I and the permeability K are dependent of the microstructures of the porous medium studied. The permeability formulation proposed by Calmidi and Mahajan[8] for ERG foams is employed in this study for Porvair foams:

$$\frac{K}{d_p^2} = 0.00073(1-\varepsilon)^{-0.224}\left(\frac{d_f}{d_p}\right)^{-1.11} \tag{3}$$

The proposed formulation for the form coefficient is

$$F_I = C\left[(1-\varepsilon)^n \big/ d_p\right] \tag{4}$$

where for FeCrAlY foams

$$C = 29.613 \qquad n = 1.5226$$

and for copper foams

$$C = 7.861 \qquad n = 0.5134$$

Additional discussion on these formulations will be presented later in the modeling section.

The thermal length scale is even more complicated in comparison with the momentum length scale because the transport of heat not only relies on the fluid behavior at the microlevel but also on the total surface area available. A proper thermal length scale should then be a combination of the momentum length scale and macrochannel height (or hydraulic diameter). However, in general, microstructural morphology details have less significant effect on overall heat transfer in comparison with macroquantities such as the total surface area. Even though the channel height does not contain any information of the porous medium used in the channel, the effect of different porous media structures on heat transfer can still be ascertained by plotting their thermal performance in one figure. Also, the overall heat transfer performance of a heat dissipation medium rather than its detailed microlevel transfer mechanism is often of primary interest for practical applications. Consequently, for simplicity, the channel height is used in this paper as the thermal length scale to define thermal quantities.

Experiment

The pressure drop and heat transfer of the six copper samples (Table 2) were measured. Similar measurements have been carried out for FeCrAlY samples, and the results were reported by Kim et al.[14] The foam was sandwiched between two 1-mm-thick copper plates using nickel-based brazing and was subsequently trimmed to fit into the test section of a heat sink channel of size 0.127 m wide × 0.127 m long × 0.012 m high.

Experimental Procedures and Measurement Uncertainty

The experimental apparatus shown in Fig. 2 consists of four sections: coolant supplier, test section, flow channel, and data acquisition system. Air at room temperature of 25°C was forced through the channel inlet by a suction type air blower. The coolant flows through a 9:1 contraction section and a flow developing channel region to ensure that the flow is hydraulically fully developed when it reaches the test section. For pressure drop measurements, the Scanivalve was calibrated with a digital micromanometer before measurements. For heat transfer experiments, an asymmetrical isoflux (constant wall heat flux) boundary condition was imposed on the lower copper plate by a heating pad (silicone–rubber etched foil from Watlow™ Inc.). To minimize heat loss from direct contact, the external surface of the heating element was covered by a 45-mm-thick Tancast 8™ thermal insulation material. A pure copper heat spreader plate (0.9 mm) was inserted between the heating element and the metal foam skin to ensure uniformity of heat flux entering the heat sink.

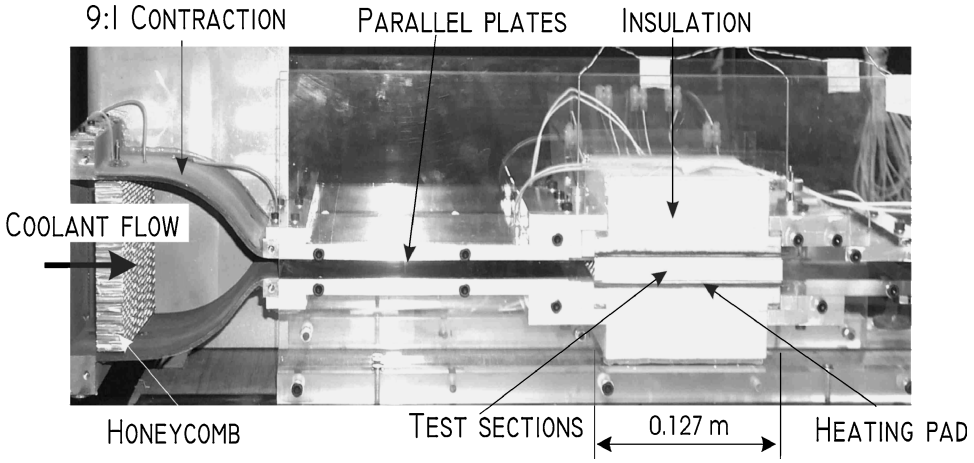

Fig. 2 Test rig for pressure drop and heat transfer experiment.

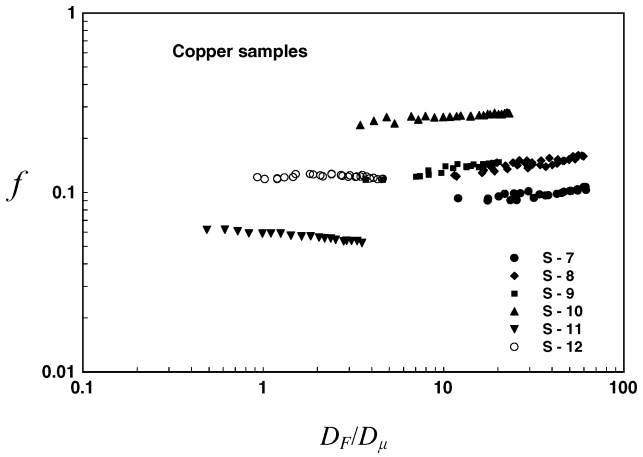

Fig. 3 Pressure drop coefficients of copper foams as functions of the ratio between form force and viscous force, D_F/D_μ.

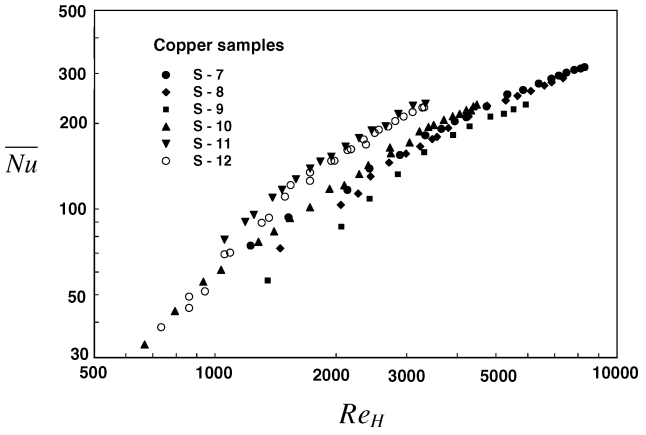

Fig. 4 Overall Nusselt number as a function of Reynolds number for copper foams.

Four thin-foil (0.05-mm-thickness) T-type copper–constantan thermocouples (from Rhopoint Inc.) were installed on the lower copper plate along the longitudinal direction, that is, the flow direction. There were two additional T-type thermocouples, positioned separately at the inlet and outlet of the test section to measure the coolant temperature at each location.

An uncertainty analysis was performed following the method of Kline and McClintock.[15] The uncertainty in the measured heat transfer coefficient and Nusselt number was calculated to be less than 7.0 and 9.6%, whereas the uncertainty in pressure drop and pressure drop coefficient measurements was obtained to be less than 5.0 and 7.8%, respectively.

Experimental Results and Discussion

Pressure Drop Coefficient

From the pressure drop measurements, the pressure drop coefficient for each sample can be calculated based on the momentum length scale L_m as

$$f = (\Delta P/\Delta L)\left[L_m\Big/\left(\rho U_m^2/2\right)\right] \tag{5}$$

where ΔP and ΔL are separately the pressure difference and distance between two pressure taps. Figure 3 shows the results of f as a function of the ratio between form force and viscous force, D_F/D_μ. Generally speaking, when $D_F/D_\mu > 10$, the flow is form dominated, and when $D_F/D_\mu < 0.1$, the flow is viscous dominated. For $0.1 < D_F/D_\mu < 10$, the viscous force and form force are both important for the hydraulic behavior. It is seen from Fig. 3 that the fluid flow is essentially in a form-dominated regime for the measured velocity range, except for samples 11 and 12, where the flow behavior is influenced by both the viscous and form forces. For a fixed cell size, the values of f for samples with 10% relative density are typically larger than those of samples with 5% relative density because the thicker solid struts in samples with higher relative densities cause larger body drag. Although the measured pressure drop across sample 12 is the largest, the same situation does not hold for the pressure drop coefficient f of Eq. (5) because of the smaller momentum length scales for samples with smaller cell sizes.

Heat Transfer

As already discussed, the channel height H is used as the thermal length scale. The thermal performance of Porvair metal foams as a heat sink medium can be assessed by calculating the overall Nusselt number defined as

$$\overline{Nu} = \frac{1}{L}\int_0^L Nu(x)\,\mathrm{d}x \tag{6}$$

where

$$Nu(x) = \{q/[T_w(x) - T_{\text{in}}]\}(H/k_f) \tag{7}$$

is the local Nusselt number at position x along the flow direction. Here, q is the applied heat flux, T_w is local substrate temperature, and $T_{\text{in}} = 25^\circ$C is the coolant inlet temperature.

The overall Nusselt number as a function of Reynolds number is plotted in Fig. 4 for all copper-foam samples. The effect of relative density on the overall heat transfer is shown in Fig. 5 for the 30 PPI samples, and the effect of cell size is presented in Fig. 6 for a fixed nominal relative density (10%). Figure 4 shows that the difference

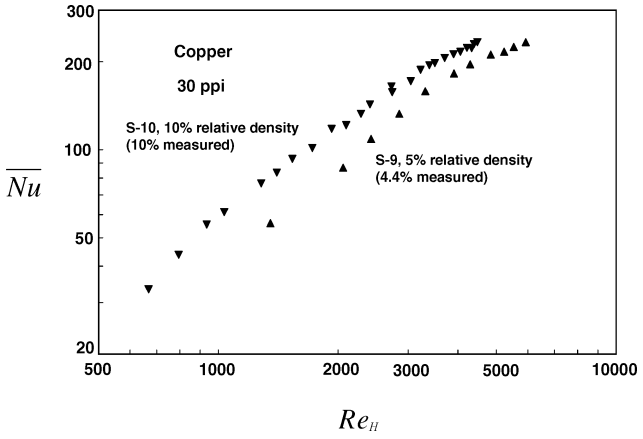

Fig. 5 Effect of relative density on overall Nusselt number of copper foams at fixed cell size of 30 PPI.

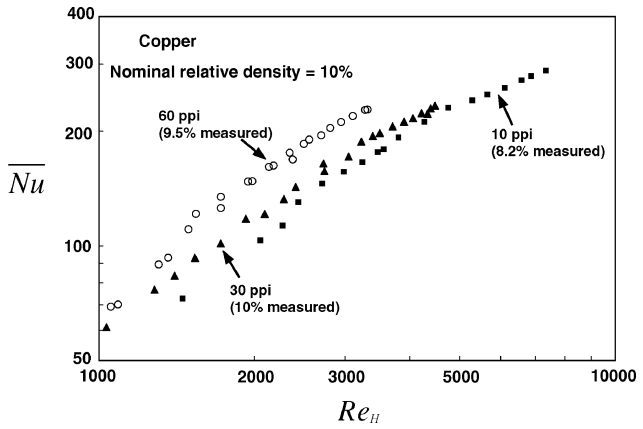

Fig. 6 Effect of cell size on overall Nusselt number of copper foams at fixed nominal relative density of 10%.

between the overall Nusselt numbers of sample 11 and sample 12 with the same nominal 60 PPI but different relative densities is small, which may be attributable to the smaller cell size for sample 11 (Table 2). From Figs. 4 and 5 and Table 2, it can be seen that the overall heat transfer of a copper sample is not as sensitive to the relative density as that for an FeCrAlY sample,[16] whereas the cell size effect on heat transfer of the copper sample is slightly more significant than that for an FeCrAlY sample.

For FeCrAlY samples, the solid thermal conductivity k_s is approximately 20 W/mK, and hence, the thermal resistance at the solid side is large. Consequently, increasing the relative density of these foams may cause significant reduction of the thermal resistance in the solid phase, resulting in a strong effect on the overall heat transfer. For copper samples, however, the solid thermal conductivity k_s is more than 300 W/mK, which implies that the thermal resistance in the solid phase is small relative to that in the fluid phase. Therefore, increasing the relative density of a copper sample would not lead to a dramatic effect on the overall heat transfer, whereas reducing the cell size could to a certain extent enhance the overall heat transfer due to the reduction of thermal resistance in the fluid phase. Figure 7 compares the thermal performance of FeCrAlY and copper samples that have the same measured relative density (10%) and PPI (30). It is seen that the slope of the Nusselt number $\overline{Nu}$ vs Reynolds number Re_H curve for the copper sample is larger than that for the corresponding FeCrAlY sample, which confirms the preceding assertion.

Modeling

The complexity of cellular morphologies typically found in commercial porous metals precludes the study of transport phenomena at the pore level. The general transport equations are usually integrated

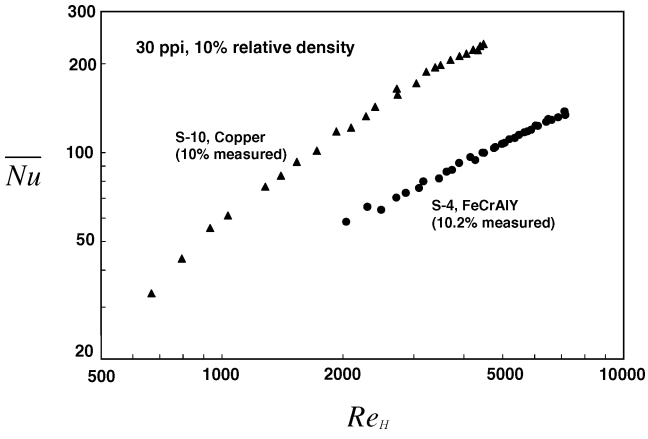

Fig. 7 Comparison of overall Nusselt number for FeCrAlY and copper samples.

over a representative elementary volume, which accommodates both the fluid and solid phases. Though the loss of information with respect to the microscopic transport phenomena is inevitable with this approach, it has been established (e.g., Refs. 8 and 12) that the integrated quantities, coupled with a set of properly established constitutive equations representing the effects of microscopic interactions on the integrated quantities, do provide a sound and effective basis for analyzing the transport phenomena in porous media.

Mathematical Formulations

The problem of concern is forced convection of incompressible fluid flow through open-celled metal foams. Because the maximum air velocity is less than 12 m/s during the experiment, the compressibility effects are estimated to be negligibly small. Because the temperature difference between the solid and fluid phases cannot be neglected in metal foams with air as the coolant fluid, the two-equation model will be employed.

Because the dimension of the channel width is 10 times the channel height, the problem can be considered as two dimensional. The other assumptions on which the analytical model is built are summarized as follows:

1) The heat transfer medium is homogeneous and isotropic.

2) Natural convection effects are negligible.

3) Variation of thermophysical properties with temperature is ignored for both the solid and fluid phases.

4) Because of the relatively low operating temperature ($<100^\circ$C) considered in the present study, radiative heat transfer is neglected.

5) Fluid flow and heat transfer are fully developed, that is, end effects are neglected.

Under these assumptions, the governing equations for velocity and temperature fields in the metal foam are established using the volume-averaging technique. The extended Darcy equation proposed by Hsu and Cheng[17] is used in place of the Darcy equation to account for the boundary and inertial effects. The governing equations and boundary conditions for the present problem are as follows.

Continuity equation:

$$\nabla \cdot \langle \boldsymbol{V} \rangle = 0 \tag{8}$$

Momentum equation:

$$(\rho_f/\varepsilon)\langle(\boldsymbol{V}\cdot\nabla)\boldsymbol{V}\rangle = -\nabla\langle P\rangle_f + \mu_f\nabla^2\langle\boldsymbol{V}\rangle - (\mu_f\varepsilon/K)\langle\boldsymbol{V}\rangle - \rho_f\varepsilon F_I[\langle\boldsymbol{V}\rangle\cdot\langle\boldsymbol{V}\rangle]J \tag{9}$$

Solid-phase energy equation:

$$0 = \nabla\cdot\{k_{se}\cdot\nabla\langle T_s\rangle\} - h_{sf}\tilde{a}(\langle T_s\rangle - \langle T_f\rangle) \tag{10}$$

Fluid-phase energy equation:

$$\langle\rho\rangle_f C_f\langle\boldsymbol{V}\rangle\cdot\nabla\langle T_f\rangle = \nabla\cdot\{k_{fe}\cdot\nabla\langle T_f\rangle\} + h_{sf}\tilde{a}(\langle T_s\rangle - \langle T_f\rangle) \tag{11}$$

In Eqs. (8–11), $\langle\ \rangle$ denotes volume averaging; $\tilde{a}$, ρ_f, μ_f, C_f, and k_{fe} are wetted area per volume, density, viscosity, heat capacity, and effective thermal conductivity of the fluid, respectively; $\boldsymbol{V}$ is the velocity vector, $J = \boldsymbol{V}_P/|\boldsymbol{V}_P|$ is the unit vector aligned along the pore velocity vector $\boldsymbol{V}_p$; and F_I is the form coefficient per meter, which depends on the microstructure of the porous medium. If the Reynolds number is small such that laminar flow prevails, $F_I = C_I/\sqrt{K}$. The second term in Eq. (9) is introduced to account for the boundary effects on velocity distribution.[18,19]

Boundary Conditions

When a uniform heat flux is directly applied to the outer surface of a metal-foam-filled plate channel, the applied heat is transferred to the solid and fluid phases by conduction and convection. As discussed in Refs. 20 and 21, the wall heat flux boundary condition may be viewed in two different ways. The first is to assume that each representative elementary volume at the wall surface receives a prescribed heat flux that is equal to the wall heat flux q_w. As a result, the heat is divided between the two phases according to their effective conductivities and temperature gradients. The second approach is to assume that each phase at the wall surface receives an equal amount of heat flux q_w (Ref. 20).

In the present study, a 1-mm copper substrate with high thermal conductivity is brazed to the metal foam as shown in Fig. 2a, and the heat flux is applied to the external wall of the copper substrate instead of being applied directly to the outer surface of the metal foam. In this case, within a representative cell, the temperature at the interface between metal foam and the substrate can be considered to be uniform, due to the high thermal conductivity of the copper cover plate, regardless of whether it is in contact with the solid or fluid phase. Consequently, the boundary condition at the heating side, $y = 0$, of the channel can be written as

$$T_f\big|_{y=0} \cong T_s\big|_{y=0} \cong T_w \tag{12}$$

where T_w is the temperature at the foam–substrate interface. This temperature is not known a priori and must be obtained as part of the solution.

Finally, the boundary conditions associated with a constant heat flux at the bottom surface of the heat sink are specified as follows.

At $y = 0$:

$$q = q_w = k_{fe}\frac{\partial T_f}{\partial y}\bigg|_{y=0} + k_{se}\frac{\partial T_s}{\partial y}\bigg|_{y=0}, \qquad T_s = T_f = T_w \tag{13a}$$

At $y = H$:

$$q = 0 \tag{13b}$$

At $x = 0$:

$$T_f = T_{in}, \qquad \frac{\partial T_s}{\partial x} = 0 \tag{13c}$$

At $x = L$:

$$\frac{\partial T_s}{\partial x} = 0, \qquad \frac{\partial T_f}{\partial x} = 0 \tag{13d}$$

The effect of replacing constant heat flux with constant wall temperature boundary condition will be examined later.

Modeling on Porvair Metal Foams

Independent Parameters

The relative density ρ_r, pore size d_p, ligament diameter d_f, and inner-to-outer ligament diameter ratio r have already been measured. It is known that these parameters are not all independent of each other. From Ref. 8, the cross relationship can be written as

$$\frac{d_f}{d_p} = 1.18\sqrt{\frac{1-\varepsilon}{3\pi}}\left(\frac{1}{1-\exp\{-[(1-\varepsilon)/0.04]\}}\right) \tag{14}$$

Note that Eq. (14) adequately describes the ERG foam morphology for which a simple relation between porosity ε and relative density ρ_r holds: $\rho_r = 1 - \varepsilon$. Thus, for ERG foams, there are only two independent foam parameters, that is, pore size d_p (or cell ligament diameter d_f) and porosity ε (or relative density ρ_r).

For Porvair foams, however, because the cell edge ligaments are hollow, another parameter, the inner-to-outer ligament diameter ratio r, is needed. The relationship between porosity and relative density then becomes

$$\rho_r = (1-\varepsilon)(1-r^2) \tag{15}$$

Consequently, the following cross relationships exist between a ERG foam and a Porvair foam: At the same porosity ε,

$$\rho_{\text{r, Porvair}} = \rho_{\text{r, ERG}}(1-r^2) \tag{16}$$

and at same relative density ρ_r,

$$\varepsilon_{\text{Porvair}} = \left(\varepsilon_{\text{ERG}} - r^2\right)\Big/(1-r^2) \tag{17}$$

Three parameters are needed to characterize a Porvair foam, namely, porosity, pore size, and inner-to-outer ligament diameter ratio. From Eq. (15), it is noted, however, that the relative density and inner-to-outer ligament diameter ratio can be integrated into one parameter, porosity. Thus, there are only two independent parameters, that is, porosity and pore size (or ligament diameter).

Permeability (K) *and Form Coefficient* (F_I)

The permeability K and form coefficient F_I appearing in Eq. (9) must be known to calculate the velocity field. Although several researchers studied the permeability of open-celled metal foams,[1,10,22,23] only Calmidi[22] gave a specific formulation for ERG foams, as

$$K\Big/d_p^2 = 0.00073(1-\varepsilon)^{-0.224}(d_f/d_p)^{-1.11} \tag{18}$$

This formulation will be adopted in this study. On the other hand, the effect of form force is significant for the velocity range studied in the present paper, being either a dominant factor for samples 7–10 or equally important with the viscous force for samples 11 and 12. The analysis of the form coefficient F_I is given next.

Dimensional analysis dictates that F_I has the reciprocal length scale, per meter. From the physical point of view, the last term in Eq. (9) is the form force caused by metal foam structures, and so it should be zero for an open channel, $\varepsilon = 1$, and inversely proportional to the pore size d_p. Consequently, based on the two independent parameters, that is, porosity ε and pore size d_p, a formulation for F_I is proposed as

$$F_I = C\left[(1-\varepsilon)^n\Big/d_p\right] \tag{19}$$

Nield[24] pointed out that the form force term (Forchheimer term) and the viscous term (Darcy term) are intrinsically linked and, hence, cannot be treated separately. From the physical point of view, the verdict should in general not be breached. However, certain mathematical treatment may be made to determine certain constants at certain occasions, for example, asymptotic cases. Because of the high Reynolds numbers studied in the present paper, the pressure drop was mainly caused by the body force; thus, from Eqs. (9) and (19), an approximate formulation for the pressure drop can be deduced as

$$-\Delta p/\Delta L = C\left[(1-\varepsilon)^n d_p\right]\rho_f u_m^2 \tag{20}$$

From Eqs. (19) and (20) the pressure drop coefficient can be obtained as

$$f = \frac{-(\Delta p/\Delta L)\cdot L_m}{\rho u_m^2/2} = 2C\,(1-\varepsilon)^n\,\frac{L_m}{d_p} \tag{21}$$

Based on experimental data, the constants C and n are for FeCrAlY foams

$$C = 29.613 \qquad n = 1.5226$$

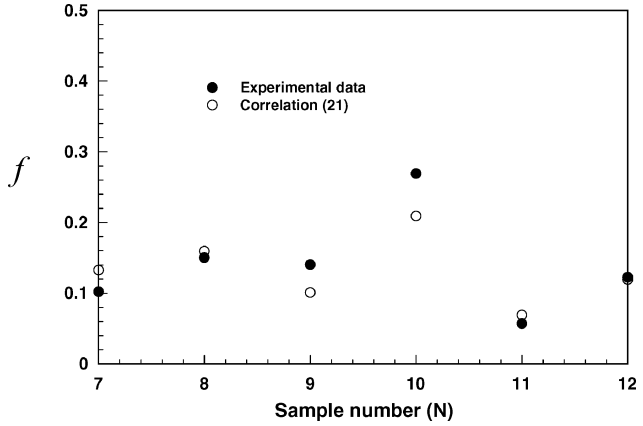

Fig. 8 Comparison between experimental results and correlation (21) for pressure drop coefficient of copper foams.

and for copper foams

$$C = 7.861 \qquad n = 0.5134$$

Figure 8 shows the comparison between correlation (21) and experimental results for copper foams. The agreement is in general good.

Kim et al.[14] measured the pressure drop and heat transfer characteristics for seven FeCrAlY foams, and the concept of K_{cell} for friction factor based on pore size was put forward. From Eq. (21), K_{cell} can be obtained as

$$K_{\text{cell}} = f_{d_p} = \frac{-(\Delta p/\Delta L)\cdot d_p}{\rho u_m^2/2} = 2C\,(1-\varepsilon)^n \tag{22}$$

It can be seen that the friction factor based on pore size is only dependent on the porosity of the metal foam.

Finally, the form coefficient F_l is determined by substituting constants C and n into Eq. (19).

Effective Thermal Conductivity

The effective solid and fluid conductivities k_{se} and k_{fe} need to be determined to close the energy equations (10) and (11). A three-dimensional analytical model for the effective conductivity of open-celled metal foams having solid struts, for example, ERG foams, was developed by Boomsma and Poulikakos.[11] With thermal radiation and air conduction neglected, this model yields

$$\frac{k_{se}}{k_s} = \frac{1}{\sqrt{2}}\left\{\frac{4\lambda}{2e^2+\pi\lambda(1-e)} + \frac{3e-2\lambda}{e^2} + \frac{\left(\sqrt{2}-2e\right)^2}{2\pi\lambda^2\left(1-2e\sqrt{2}\right)}\right\}^{-1} \tag{23}$$

where $e = 0.339$ and

$$\lambda = \sqrt{\frac{\sqrt{2}\left[2-\left(\frac{5}{8}\right)e^3\sqrt{2}-2\varepsilon\right]}{\pi\left(3-4e\sqrt{2}-e\right)}} \tag{24}$$

and ε is the porosity of the foam having solid cell ligaments. For Porvair foams with hollow cell ligaments, the porosity and effective solid conductivity need to be changed accordingly. If the Porvair foam has the same relative density as the ERG foam, its porosity can be calculated according to

$$\varepsilon_{\text{Porvair}} = (\varepsilon - r^2)/(1-r^2) \tag{25}$$

Similarly, because the effective solid conductivity of a foam is linearly proportional to the relative density, it can be calculated as

$$k_{se,\,\text{Porvair}} = k_{se}(1-r^2) \tag{26}$$

Surface Area Density ã *and Interstitial Heat Transfer Coefficient* h_{sf}

The surface area density $\tilde{a}$ and interstitial heat transfer coefficient h_{sf} are obtained by approximating the cellular foam structure with idealized interconnected cylinders.[5,8,11] The solid–fluid interfacial surface area for arrays of parallel cylinders intersecting in three mutually perpendicular directions is[8]

$$\tilde{a} = 3\pi d_f \big/ d_p^2 \tag{27}$$

For h_{sf}, Wakao et al.[25] proposed one of the most comprehensive models for packed beds. For foamed materials, however, no such general model exists. Because the highly porous metal foam exhibits somewhat similar microstructures to a bank of staggered cylinders, it is assumed that the correlation developed by Zukauskas[26] for staggered cylinders in crossflow may be employed,

$$h_{sf} = C_T Re^{0.5} Pr^{0.37} k_f \big/ d_f \tag{28}$$

where $Re = ud_f/(\varepsilon\nu)$ is based on fluid velocity near the cell ligament and $C_T = 0.52$.

Numerical Procedures

The combined continuity, momentum, and energy equations are solved numerically with the SIMPLE algorithm.[27] The control-volume formulation utilized in this algorithm ensures the continuity of convective and diffusive fluxes, as well as overall momentum and energy conservation. The harmonic mean formulation adopted for the interface diffusion coefficients between two control volumes can handle abrupt changes in these coefficients. For all of the cases studied, it is found that a uniform grid of 127×46 used in the x and y directions can ensure the mesh independence of the solution. The governing equations were solved by using the alternate direction iteration numerical scheme. The iteration is terminated when changes in target variables u, v, T_s and T_f are less than 10^{-5} between successive iterations.

Numerical Results for Porvair Metal Foams

Although numerical calculations have been carried out for all foam samples listed in Tables 1 and 2, here only the results for selected foam samples may given results on the rest of the samples may be found in Ref. 16. The predicted overall Nusselt numbers $\overline{Nu}$ as a function of Reynolds number Re_H are plotted in Fig. 9 for FeCrAlY sample 1 and for copper sample 7; the solid lines represent predictions based on the solid conductivity $k_s = 16$ W/mK for FeCrAlY and $k_s = 372$ W/mK for copper. For comparison, the corresponding experimental data are also included. Given the complexity of heat transfer in metal foams, the predictions appear to be in reasonable agreement with those measured, although the prediction somewhat underestimates the Nusselt number for FeCrAlY foams and overestimates the overall heat transfer rate for copper foams. The reason may be attributed to the effect of nickel-based brazing

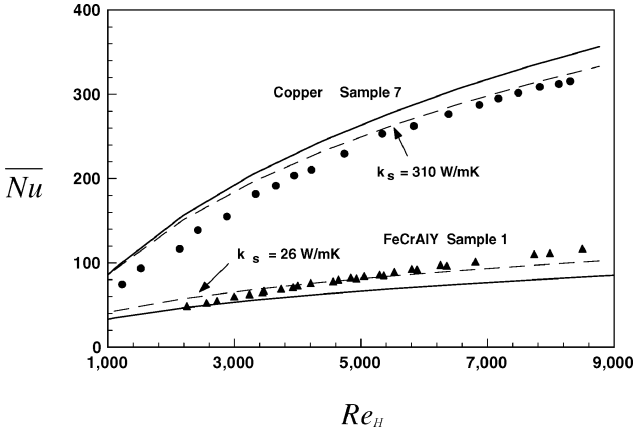

Fig. 9 Comparison between numerical predictions and experimental results.

on the solid conductivity k_s. Brazing may increase the solid conductivity for FeCrAlY samples and decrease the solid conductivity for copper samples. In Fig. 9, the dashed lines represent predictions obtained by changing the solid conductivity for both FeCrAlY and copper, with the rest of the parameters remaining unchanged. It was found that a solid conductivity ranging from 20 to 26 W/mK for different FeCrAlY samples and from 300 to 320 W/mK for different copper samples led to improved predictions in comparison with the test data. Similar trends were observed for other samples listed in Tables 1 and 2 (Ref. 16).

Effects of Foam Parameters

In this section, the experimentally verified analytical model is used to study the effects of key parameters such as solid conductivity, pore size, and porosity on forced air convection in metal foams. By the consideration of the balance between overall heat transfer and pressure drop, optimal foam morphology, if it exists, will then be identified.

Solid Thermal Conductivity

The effect of solid conductivity k_s on the overall Nusselt number is shown in Fig. 10 for a fixed microstructure (sample 4) and selected values of the Reynolds number. The results reveal that the overall Nusselt number increases sharply with increasing k_s when k_s is small and then gradually approaches a plateau as k_s is further increased. For small Reynolds numbers, for example, $Re_H = 600$, heat transfer saturation occurs at small thermal conductivity levels ($k_s \approx 50$ W/mK), whereas for large Reynolds numbers, for example, $Re_H = 2200$, the overall heat transfer reaches saturation when $k_s \approx 200$ W/mK. This implies that the main thermal resistance for small Reynolds numbers lies on the fluid side when k_s exceeds a critical value ($\approx$50 W/mK). Here, we define this value as $k_{s,\max}$, beyond which the overall Nusselt number is independent of solid thermal conductivity. For higher Reynolds numbers, $k_{s,\max}$ becomes larger because the thermal resistance in the fluid side decreases. Consequently, in practical applications, it appears that there is no need to use foam materials with high thermal conductivities if the Reynolds number is small.

Porosity

With $r = 0$ assumed, the relationship between porosity and relative density can be simplified as $\rho_r = 1 - \varepsilon$. It has been established that the overall Nusselt number decreases as the porosity is increased (at a fixed fiber diameter). In other words, the transport of heat is enhanced by increasing the relative density of the foam, although this is accompanied by the penalty of increasing drag resistance. With $r = 0$ and $d_f = 0.4$ mm, the thermal efficiency index $\tilde{I} = \overline{Nu} L_m/(fH)$ is plotted as a function of porosity in Fig. 11a for selected values of the Reynolds number. For a given Reynolds number, there exists an optimized porosity ε_{opt}, which maximizes the efficiency index (Fig. 11a). However, this optimized porosity is not independent of the Reynolds number; it decreases with increasing Reynolds number Re_H. The variation of ε_{opt} with Reynolds number Re_H is shown in Fig. 11b for three different fiber diameters: $d_f = 0.1$, 0.2, and 0.4 mm. The optimized porosity ε_{opt} decreases with increasing fiber diameter, particularly so for large Reynolds numbers. For the range of Reynolds number of practical interest, the optimal porosity varies from 0.85 to 0.95, corresponding to a relative density of between 0.5 and 0.15.

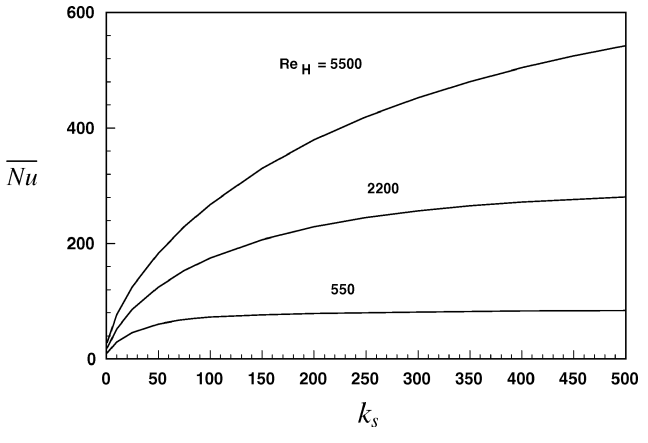

Fig. 10 Effect of solid conductivity on overall Nusselt number.

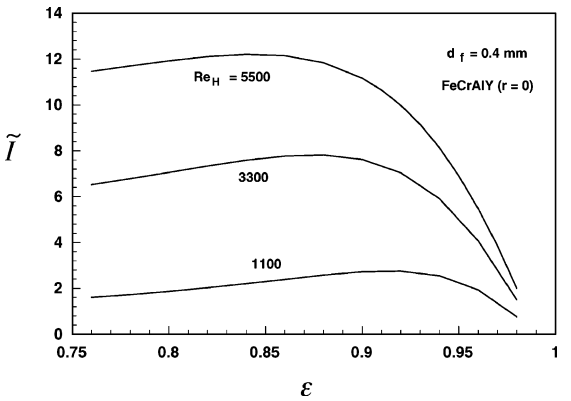

Fig. 11a Effect of porosity ε on thermal efficiency index $\tilde{I}$.

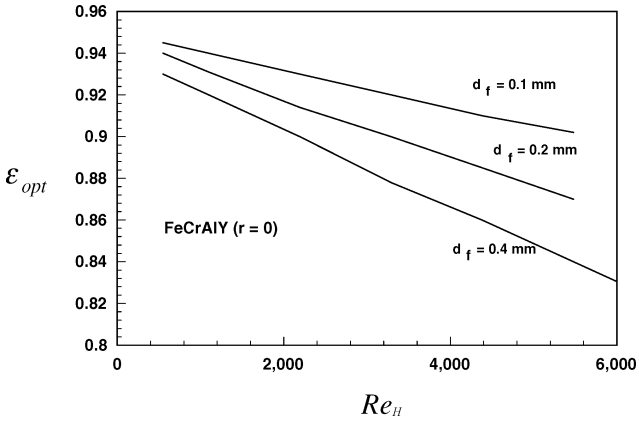

Fig. 11b Variation of optimal porosity ε_{opt} with Reynolds number.

Conclusions

The morphologies of FeCrAlY and copper foams were quantified with the SEM and image analysis software, and it was found that the measured foam parameters are significantly different from industrial specifications. A detailed experimental study of forced air convection across copper foams was subsequently carried out. The results indicate that heat transfer in copper foams is more sensitive to cell size than relative density, whereas the reverse is true for FeCrAlY foams.[13,15] This can be attributed to the different thermal resistances in the solid side for FeCrAlY and copper foams. The heat dissipation capability of both foams increases with increasing relative density and decreases with increasing cell size.

Independent parameters characterizing open-celled metal foams with hollow cell edge ligaments were determined. The momentum equation was reexamined and a formulation on the nonlinear term based on foam microstructures was proposed for high Reynolds numbers. A numerical model incorporating the measured foam parameters was developed for forced air convection in metal foams. Reasonably good agreement between prediction and measurement is achieved. The effects of solid conductivity and porosity on the overall heat transfer performance of a foam-filled channel were investigated. An optimal foam porosity ε_{opt} is identified by considering the balance between pressure drop and heat transfer, and the results show that ε_{opt} decreases as the Reynolds number is increased.

Acknowledgments

This work is supported partly through Office of Naval Research/ Office of Naval Research International Field Office Grant N000140110271 and Office of Naval Research Grant N000140210117, partly by Engineering and Physical Scientific Research Council Grant EJA/U83, and partly by Porvair Fell Cell Technology.

References

[1]Hunt, M. L., and Tien, C. L., "Effects of Thermal Dispersion on Forced Convection in Fibrous Media," *International Journal of Heat and Mass Transfer*, Vol. 31, No. 2, 1988, pp. 301–309.

[2]Sathe, S. B., Peck, R. E., and Tong, T. W., "A Numerical Analysis of Heat Transfer and Combustion in Porous Radiant Burners," *International Journal of Heat and Mass Transfer*, Vol. 33, No. 6, 1990, pp. 1331–1338.

[3]Younis, L. B., and Viskanta, R., "Experimental Determination of the Volumetric Heat Transfer Coefficient Between Stream of Air and Ceramic Foam," *International Journal of Heat and Mass Transfer*, Vol. 36, No. 6, 1993, pp. 1425–1434.

[4]Lee, Y. C., Zhang, W., Xie, H., and Mahajan, R. L., "Cooling of a FCHIP Package with 100 w, 1 cm^2 chip," *Proceedings of the 1993 ASME International Electronic Packaging Conference*, Vol. 1, American Society of Mechanical Engineers, New York, 1993, pp. 419–423.

[5]Lu, T. J., Stone, H. A., and Ashby, M. F., "Heat Transfer in Open-Celled Metal Foams," *Acta Mater*, Vol. 46, No. 10, 1998, pp. 3619–3635.

[6]Bastarows, A. F., Evans, A. G., and Stone, H. A., "Evaluation of Cellular Metal Heat Dissipation Media," Technical Rept. MECH-325, Division of Engineering and Applied Sciences, Harvard Univ., Cambridge, MA, 1998.

[7]Calmidi, V. V., and Mahajan, R. L., "The Effective Thermal Conductivity of High Porosity Fibrous Metal Foams," *Journal of Heat Transfer*, Vol. 121, No. 2, 1999, pp. 466–471.

[8]Calmidi, V. V., and Mahajan, R. L., "Forced Convection in High Porosity Metal Foams," *Journal of Heat Transfer*, Vol. 122, No. 3, 2000, pp. 557–565.

[9]Kim, S. Y., Paek, J. W., and Kang, B. H., "Flow and Heat Transfer Correlations for Porous Fin in a Plate–Fin Heat Exchanger," *Journal of Heat Transfer*, Vol. 122, No. 3, 2000, pp. 572–578.

[10]Paek, J. W., Kang, B. H., Kim, S. Y., and Hyun, J. M., "Effective Thermal Conductivity and Permeability of Aluminium Foam Materials," *International Journal of Thermophysics*, Vol. 21, No. 3, 2000, pp. 453–464.

[11]Boomsma, K., and Poulikakos, D., "On the Effective Thermal Conductivity of a Three-Dimensionally Structured Fluid-Saturated Metal Foam," *International Journal of Heat and Mass Transfer*, Vol. 44, No. 4, 2001, pp. 827–836.

[12]Zhao, C. Y., Kim, T., Lu, T. J., and Hodson, H. P., "Modeling on Thermal Transport in Cellular Metal Foams," AIAA Paper 2002-3014, June 2002.

[13]Lage, J. L., "The Fundamental Theory of Flow Through Permeable Media from Darcy to Turbulence," *Transport Phenomena in Porous Media*, edited by D. B. Ingham and I. Pop, Pergamon, Oxford, 1998, pp. 1–30.

[14]Kim, T., Fuller, A. J., Hodson, H. P., and Lu, T. J., "An Experimental Study on Thermal Transport in Lightweight Metal Foams at High Reynolds Numbers," *Proceedings of the International Symposium of Compact Heat Exchangers*, AIAA, Reston, VA, 2002, pp. 227–232.

[15]Kline, S. J., and McClintock, F. A., "Describing Uncertainties in Single-Sample Experiments," *Mechanical Engineering*, Vol. 75, No. 1, 1953, pp. 3–8.

[16]Zhao, C. Y., Kim, T., Lu, T. J., and Hodson, H. P., "Thermal Transport Phenomena in Porvair Metal Foams and Sintered Beds," Engineering Dept. Rep. 2031, Cambridge Univ., Cambridge, England, U.K., Aug. 2001.

[17]Hsu, C. T., and Cheng, P., "Thermal Dispersion in a Porous Medium," *International Journal of Heat and Mass Transfer*, Vol. 33, No. 8, 1990, pp. 1587–1597.

[18]Vafai, K., and Tien, C. L., "Boundary and Inertial Effects on Flow and Heat Transfer in Porous Media," *International Journal of Heat and Mass Transfer*, Vol. 24, No. 2, 1981, pp. 195–203.

[19]Vafai, K., and Sozen, M., "Analysis of Energy and Momentum Transport for Fluid Flow Through a Porous Bed," *Journal of Heat Transfer*, Vol. 112, No. 3, 1990, pp. 690–699.

[20]Lee, D. Y., and Vafai, K., "Analytical Characterization and Conceptual Assessment of Solid and Fluid Temperature Differentials in Porous Media," *International Journal of Heat and Mass Transfer*, Vol. 42, No. 3, 1999, pp. 423–435.

[21]Amiri, A., Vafai, K., and Kuzay, T. M., "Effects of Boundary Conditions on Non-Darcian Heat Transfer Through Porous Media and Experimental Comparisons," *Numerical Heat Transfer*, Pt. A, 1995, pp. 651–664.

[22]Calmidi, V. V., "Transport Phenomena in High Porosity Fibrous Metal Foams," Ph.D. Dissertation, Dept. of Mechanical Engineering, Univ. of Colorado, CO, July 1998.

[23]Ngo, N. D., and Tamma, K. K., "Microscale Permeability Predictions of Porous Fibrous Media," *International Journal of Heat and Mass Transfer*, Vol. 44, No. 16, 2001, pp. 3135–3145.

[24]Nield, D. A., "Modelling Fluid Flow in Saturated Porous Media and at Interfaces," *Transport Phenomena in Porous Media II*, edited by D. B. Ingham and I. Pop, Pergamon, Elsevier Science, Oxford, 2002, pp. 1–19.

[25]Wakao, N., Kaguei, S., and Funazkri, T., "Effect of Fluid Dispersion Coefficient on Particle-to-Fluid Heat Transfer Coefficients in Packed Beds," *Chemical Engineering Science*, Vol. 34, No. 3, 1979, pp. 325–336.

[26]Zukauskas, A. A., "Convective Heat Transfer in Cross-Flow," *Handbook of Single-Phase Heat Transfer*, Wiley, New York, 1987, Chap. 6.

[27]Patankar, S., *Numerical Heat Transfer and Fluid Flow*, Hemisphere, New York, 1980, Chap. 6.